

# Pedestrian Dead Reckoning Based on Walking Pattern Recognition and Online Magnetic Fingerprint Trajectory Calibration

Qu Wang<sup>1</sup>, Member, IEEE, Haiyong Luo<sup>1</sup>, Member, IEEE, Hao Xiong, Aidong Men, Member, IEEE, Fang Zhao<sup>2</sup>, Ming Xia<sup>3</sup>, and Changhai Ou<sup>1</sup>

**Abstract**—With the explosive development of pervasive computing and the Internet of Things (IoT), indoor positioning and navigation have attracted immense attention over recent years. Pedestrian dead reckoning (PDR) is a potential autonomous localization technology that obtains position estimation employing built-in sensors. However, most existing PDR methods assume that the smartphone is held horizontally and points to the walking direction. To solve reckoning errors caused by inconsistency of headings between walking heading and pointing of smartphone, we design an accurate and robust PDR method based on walking patterns, which is identified by multihead convolutional neural networks. In addition to adaptively adjust the threshold of step detection and select the most suitable step length model according to the results of walking pattern recognition, a novel heading estimation approach independent of device orientation is proposed. To mitigate accumulative errors, we proposed an online trajectory calibration method based on forward and backward magnetic fingerprint trajectory matching. We conduct extensive and well-designed experiments in typical scenarios, and

Manuscript received April 20, 2020; revised June 18, 2020; accepted August 9, 2020. Date of publication August 12, 2020; date of current version January 22, 2021. This work was supported in part by the National Key Research and Development Program under Grant 2018YFB0505200; in part by the Action Plan Project of the Beijing University of Posts and Telecommunications supported by the Fundamental Research Funds for the Central Universities under Grant 2019XD-A06; in part by the Special Project for Youth Research and Innovation, Beijing University of Posts and Telecommunications; in part by the Fundamental Research Funds for the Central Universities under Grant 2019PTB-011; in part by the National Science Foundation of China under Grant 61872046, Grant 61671264, and Grant 61671077; in part by the Joint Research Fund for Beijing Natural Science Foundation and Haidian Original Innovation under Grant L192004; in part by the Key Research and Development Project from Hebei Province under Grant 19210404D; in part by the BUPT Excellent Ph.D. Students Foundation under Grant CX2020306; and in part by the Open Project of the Beijing Key Laboratory of Mobile Computing and Pervasive Device. (Corresponding authors: Haiyong Luo; Aidong Men.)

Qu Wang and Aidong Men are with the School of Information and Communication Engineering, Beijing University of Posts and Telecommunications, Beijing 100876, China (e-mail: wangqu@ict.ac.cn; menad@bupt.edu.cn).

Haiyong Luo is with the Beijing Key Laboratory of Mobile Computing and Pervasive Device, Institute of Computing Technology, Chinese Academy of Sciences, Beijing 100190, China (e-mail: yhluo@ict.ac.cn).

Hao Xiong and Fang Zhao are with the School of Software Engineering, Beijing University of Posts and Telecommunications, Beijing 100876, China (e-mail: xmr2015211989@bupt.edu.cn; zfsse@bupt.edu.cn).

Ming Xia is with the School of Electronic and Information Engineering, Beihang University, Beijing 100191, China (e-mail: xiaming@buaa.edu.cn).

Changhai Ou is with the School of Computer Science and Engineering, Nanyang Technological University, Singapore 639798 (e-mail: chou@ntu.edu.sg).

Digital Object Identifier 10.1109/JIOT.2020.3016146

the experimental results indicate that the 75th percentile localization accuracy of the three scenarios is 1.06, 1.08, and 1.22 m, respectively, using the commercial smartphone embedded sensor without any dedicated infrastructures or training data. Despite the intricate pedestrian locomotion, the proposed PDR method has great potential in pedestrian positioning.

**Index Terms**—Heading estimation, indoor positioning, Internet of Things (IoT), online calibration, pedestrian dead reckoning (PDR), walking pattern recognition.

## I. INTRODUCTION

AS A CORE technology of the Internet of Things, accurate and pervasive location-based service significantly facilitates our daily life. The latest market research predicts that the market size of global indoor location-based services is expected to reach \$18.74 billion by 2025, rising at a compound average growth rate (CAGR) of 37.8% [1]. There is a great demand for effective indoor location-based services. However, the global positioning system (GPS) signals cannot cover many indoor scenarios, for instance, shopping malls, underground parking lots, and museums.

To provide indoor location-based services, many types of indoor positioning and tracking technologies have been proposed, including RFID [2], ZigBee, UWB [3], Bluetooth [4], Wi-Fi [5], [6], visible light [7], [8], and magnetic field [9]–[12]. These technologies are classified into ranging-based methods and fingerprint-based methods. Ranging-based methods convert the received signal strength values to the distances between smartphone and reference points, then a trilateral or multilateral positioning algorithm is used to estimate pedestrian position. Positioning performance depends on the deployment density of the base station. Additional positioning dedicated base stations increase system application costs. Moreover, the wireless signal is susceptible to the effect of multipath propagation. The fingerprinting method obtains position estimation by comparing online radio features with a precollected radio map. The accuracy of fingerprint-based positioning methods is susceptible to the effect of device orientation, pedestrians, removing or adding furniture, and layout changes. Moreover, localization accuracy relies on the density of the fingerprint observation points, as well as the collection and maintenance

of a high-quality radio map are time-consuming and labor-intensive processes. Furthermore, radio-frequency signals are prohibited in electromagnetic-sensitive scenarios such as mines due to its safety concerns. Both fingerprint-based and specialized infrastructure-based positioning methods are not suitable for emergency scenarios, such as fire rescues, which are hard to preinstall specific infrastructures or collect training fingerprints.

Inertial navigation is an autonomous localization method that obtains position estimation without any dedicated infrastructures and training fingerprints, has spawned extensive applications in the emergency rescue (positioning and tracking firefighters and survivors in the fire) and anti-terrorism action [13]. In addition to emergency rescue, inertial navigation is widely used in location-based services in smart spaces (e.g., shopping malls and airports), healthcare in the hospitals, or at home (e.g., for tracking locations and analyzing activities of patients and older people).

Today, inertial navigation technologies are classified into strapdown inertial navigation system (SINS) and pedestrian dead reckoning (PDR). SINS binds one or more inertial measurement units (IMUs) human body (such as head, waist, legs, feet, etc.), utilizes the mechanical equation to calculate the location of pedestrians, and employs zero velocity update (ZUPT) to reset the integration errors. However, special binding devices to the body not only increase additional burden but also increase costs. Binding special devices is inconvenient in many scenarios. PDR calculates walking steps and estimates step length and moving direction based on the smartphone-embedded IMUs to reckon the position of pedestrian. Getting rid of the constraints of special binding devices to the body, PDR usually uses accompanied smartphone to estimate the location of the pedestrian with higher portability.

The most existing PDR methods assume that the smartphone is held horizontally and is oriented in a direction consistent with the walking direction. They do not consider backward or lateral movements. These methods perform well under forward walking. However, the walking pattern is random and varied, including many abnormal walking patterns, such as backward walking and lateral walking. The existing PDR algorithms easily encounter problems in intricate walking patterns. As shown in Fig. 1, since the heading of PDR represents the pedestrian's walking direction, not the smartphone pointing, different walking patterns will cause wrong moving heading estimation. Because of the inconsistency of headings between walking heading and pointing of smartphone, different walk patterns require different strategies to reckon the position of the pedestrian.

To solve reckoning errors caused by the inconsistency of headings between walking heading and pointing of smartphone, we design an accurate and robust PDR method based on the walking pattern just employing a smartphone. To mitigate accumulative errors, we proposed an online trajectory calibration method based on forward and backward magnetic fingerprint trajectory matching.

The key contributions of our study are as follows.

- 1) We propose a walking pattern recognition method based on a multihead convolutional attention mechanism. The

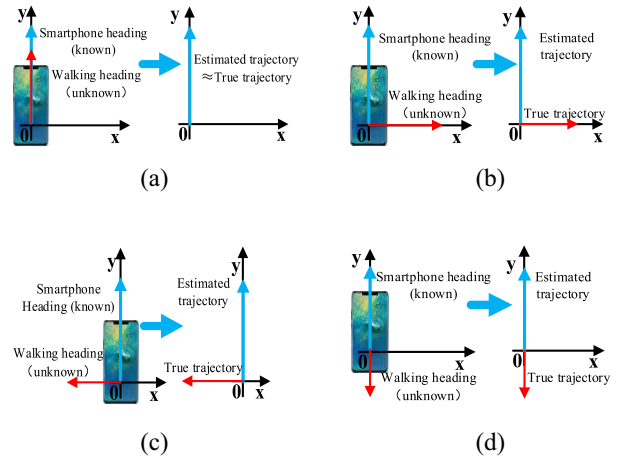


Fig. 1. Navigation error due to walking patterns. (a) Forward walking. (b) Right lateral walking. (c) Left lateral walking. (d) Backward walking.

multihead attention mechanism is used to learn the relevance of time-series features captured by convolutional neural networks (CNNs).

- 2) We propose a PDR based on walking pattern recognition. In addition to adaptively adjust the threshold of step detection and select the most suitable step length model according to the results of walking pattern recognition, a novel heading estimation approach independent of device orientation is proposed.
- 3) We construct attitude-free 3-D forward and backward magnetic fingerprint trajectory, and leverage opportunistic online magnetic loop closures to calibrate the position and moving direction of pedestrian, thus restraining the PDR positioning error accumulation.
- 4) We conduct extensive well-designed experiments in typical scenarios to evaluate and analyze the accuracy of our proposed method and achieve satisfactory accuracy. Since the independence of infrastructure and historical data, the proposed PDR method is easy to integrate with any applications that require accurate location-based services.

The remainder of this article is organized as follows. Section II reviews the related literature. Section III illustrates the proposed PDR method based on walking pattern recognition and online magnetic fingerprint trajectory calibration. Section IV evaluates the proposed method. Finally, Section V draws a conclusion.

## II. RELATED WORK

We review the related literature of pedestrian motion modes recognition, PDR, and pedestrian trajectory calibration.

### A. Pedestrian Motion Modes Recognition

Pedestrian motion modes recognition is an essential topic in the health, computer vision, and positioning and navigation field because it has many applications, including human activity recognition, prediction of human health status, sports training, and human-computer interaction. Generally, pedestrian motion modes recognition methods are classified into

vision-based methods and sensor-based methods. Vision-based motion modes recognition obtains high recognition accuracy, but it causes high-power consumption and privacy problems. This study focuses on pedestrian motion recognition using smartphone embedded sensors (accelerometer, gyroscope, or barometer) to recognize pedestrian motion modes.

Plenty of studies on pedestrian motion modes recognition using the IMUs have been developed. Pei *et al.* [14] extracted the 27 features by employing the raw observations from the accelerometer and magnetometer embedded in the smartphone to recognize eight motions. Ronao and Cho [15] proposed an efficient and effective pedestrian motion modes recognition algorithm using sensors built-in smartphone, in which a deep CNN was performed to exploit the inherent characteristics of motions and 1-D time-series signals. Zhang *et al.* [16] employed multihead convolution neural networks integrated with attention to recognize various motions, including walking, standing, sitting, jogging, upstairs, and downstairs. Gao *et al.* [17] recognized human activities based on stacking denoising autoencoder and lightGBM. To address the imbalanced distribution issue of labeled data over classes, Chen *et al.* [18] proposed a pattern-balanced semisupervised framework based on recurrent convolutional attention networks to extract features and recognize diverse latent motion patterns. Saeed *et al.* [19] proposed multitask self-supervised learning to recognize human activities. AROMA [20] leveraged deep multitask learning to recognize simple and complex activities.

### B. Pedestrian Dead Reckoning

Extensive studies on PDR have been developed. A typical PDR system contains three components: 1) step detection; 2) step length estimation; and 3) heading estimation.

The first step of PDR is step detection, which is used to determine the data interval required to estimate step length and heading of the pedestrian at each step. An ocean of studies on step detection and step counting have been done, categorizing into the following groups: threshold setting [21] and peak detection method [22], correlation method [23], spectral analysis method, and machine learning [24]. However, these algorithms' performance is highly sensitive to pedestrian walking patterns.

Methods of estimating pedestrian step length based on inertial sensors are summarized as three categories: 1) double integration method of acceleration; 2) models or assumptions methods; and 3) deep learning methods [25]. Step length estimation based on double integration does not rely on any individual information [26]. However, the nonnegligible drift and noise of inertial sensors resulted in the motion distance estimation error accumulating boundless with time [26]. Considerable step length estimation studies based on model or assumption are summarized as biomechanical models [27], linear models [28], nonlinear models [29], and inverted pendulum model [30]. Additionally, some researchers leveraged

the regression-based method [31], [32] and the deep-learning-based method [25], [33], [34] to predict the walking distance of pedestrian.

Based on the fact that acceleration and magnetic field provide absolute heading whereas angular rates produce relative heading by integrating iteratively, most smartphones-based heading estimation methods estimate pedestrian heading by fusing acceleration data, angular rates data, and magnetic field data. To estimate heading, attitude and heading reference systems (AHRSs) [35] leveraged the gradient-descent algorithm and complementary filter to combine inertial sensors and magnetometer observations. Kang and Han [36] built a weighted model to fuse the IMUs outputs for heading estimation. To obtain more accurate heading, numerous studies utilized extended Kalman filtering and complementary filters to fuse accelerometers, gyroscopes, and magnetometer readings, and reduce sensor noise. Because of the inconsistency of pedestrian coordinate frames and device coordinate frames, different smartphone carrying modes require different methods to estimate pedestrian walking heading. To address this issue, some studies [37]–[41] focus on heading estimation under different smartphone carrying modes, and leverage the principal component analysis (PCA) or enhanced PCA algorithm to extract the largest variations of the horizontal accelerations for heading estimation [42]. In our previous work [43], we leverage the spatial transformer networks to align the navigation coordinate system (NCS) and the body coordinate system (BCS), then designed a hierarchical LSTM-based Seq2Seq heading model to estimate the walking heading of the pedestrian. Despite its importance, heading estimation is still an open issue in PDR.

With the three components above, the position of the pedestrian is estimated through accumulating displacements. However, smartphone-embedded low-cost sensors lack factory calibration so that the measurements are easily contaminated by hard or soft iron error, bias error, and scale factor errors. The contaminated measurements result in significant errors in each of the three components in PDR, which causes accumulative errors increasing with walking distance and time. Moreover, most PDR algorithms require that pedestrian holds smartphone horizontally and points to the walking heading, which limits the practicability of PDR. Therefore, providing an accurate and robust location-based service just employing a smartphone in the intricate walking pattern is still an open challenge and needs to be resolved urgently.

### C. Trajectory Calibration

Numerous improved methods have been developed to mitigate the accumulative errors of PDR systems. A low-pass filter is applied to reduce the random noise of sensor measurements [36], [44]. Landmark calibration is a common and effective way to eliminate accumulative errors. Magnago *et al.* [45] leveraged the camera to capture the optimal image landmarks. However, image feature extraction and matching caused high-power consumption and privacy problems. Shang *et al.* [46] regarded the location of the pedestrian performed different activities as a landmark and

then utilized these landmarks to calibrate the PDR error. Kim and Kim [47] leveraged statistical methods to recognize turning points, stairs according to the sensors data from accelerometers, magnetometers, and gyroscope. Liu *et al.* [48] integrated visual and inertial information to recognize special spatial structures (e.g., intersections, corridors, or corners) by using a Bayesian classifier to prevent the accumulative error. Zhou *et al.* [49] recognized nine types of activities, including still, walk, upstairs, up elevator, up escalator, down elevator, down escalator, downstairs, and turning, then utilized activity sequence-based map matching to calibrate the PDR error. Once detecting the repetitive landmark during walking, accumulative errors derived from PDR would be calibrated. However, it is difficult to capture the steady sensor features and effectively recognize each landmark under intricate walking patterns.

Some researches leveraged Kalman filter or particle filter methods to fuse opportunistic signals, such as global positioning system (GPS) [50], RFID, Wi-Fi [9], [51], magnetic [7], Bluetooth [4], or visible Light [8] for calibrating accumulative errors. Hölzke *et al.* [50] leveraged GPS to provide initial position and reduce accumulative errors of PDR. However, GPS signals are often unlocked and not enough to provide calibration for PDR in most indoor environments. Shen and Hui [51] utilized the received signal strength indicator (RSSI) of Wi-Fi and the corresponding base station locations to correct the walking heading and enhance PDR accuracy. To obtain accurate position estimation, Wang *et al.* [52] analyzed the variations of Wi-Fi RSSI and defined several kinds of indoor landmarks. To restrain the accumulative error of PDR, DRBMs [4] utilized Kalman filter to fuse the Bluetooth ranging localization results and PDR. Based on map constraints, Xia *et al.* [53] used RSSI values of iBeacon devices as observations in the particle to reckon the position of pedestrian. Li *et al.* [54] designed a three-level quality control (QC) mechanism to fuse the localization results of PDR, Wi-Fi fingerprinting, and magnetic matching. Wang *et al.* [7] leveraged the combination fingerprinting of magnetic and visible light to calibrate the step length, heading, and position error of pedestrian via the particle filter.

These approaches mentioned above significantly improve the accuracy of PDR with the assistance of historical training data or other external devices, rather than enhancing the PDR algorithm itself. These methods not only increase the deployment cost and signal fingerprinting maintenance cost but also disrupt self-contained of the PDR system. If the pedestrian walks in a new region without historical training data or other preinstalled assisted localization devices, the localization performance of PDR will dramatically degrade or even loses the ability of localization.

### III. MATERIALS AND METHODS

#### A. System Architecture

In this study, we determine the walking pattern by a multi-head convolutional attention network. Subsequently, we propose a walking pattern-based PDR method that adaptively adjusts parameters of step detection and step length estimation, estimates pedestrian heading for arbitrary smartphone-hold

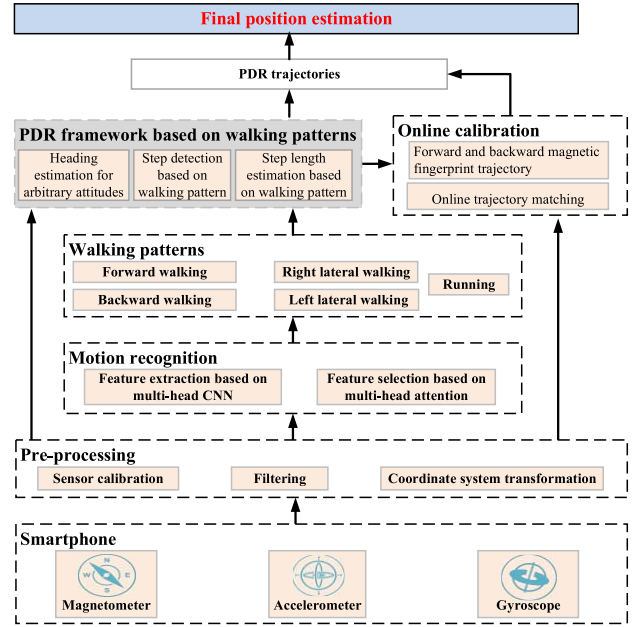


Fig. 2. System architecture of the proposed PDR method based on walking pattern recognition.

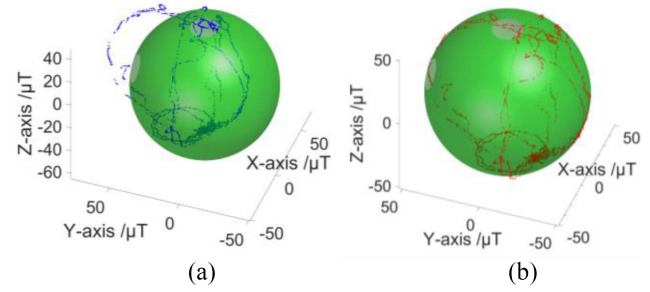


Fig. 3. Magnetometer calibration. (a) Uncalibrated. (b) Calibrated.

attitude and updates the position of pedestrian according to the walking pattern. Furthermore, we leverage the online magnetic fingerprint trajectory to calibrate the position and moving direction error of the pedestrian (see Fig. 2).

#### B. Magnetometer Calibration

The low-cost magnetometer embedded in the smartphone is easily disturbed by other magnetic sources, such as electronic devices and ferrous materials. Therefore, magnetometer error calibration is necessary when using the measurements of the magnetometer to estimate the heading of the pedestrian. We leverage ellipsoid fitting [55] to calibrate the measurement errors. The errors are estimated through the ellipsoid equation that is expressed as follows:

$$k_x^2(m_x - e_x)^2 + k_y^2(m_y - e_y)^2 + k_z^2(m_z - e_z)^2 = R^2 \quad (1)$$

where  $k_x$ ,  $k_y$ , and  $k_z$  denote the scale factors of the magnetometer;  $m_x$ ,  $m_y$ , and  $m_z$  denote the raw measurements of the magnetometer in BCS;  $e_x$ ,  $e_y$ , and  $e_z$  denote the offset caused by hard-iron distortion; and  $R$  denotes the magnitude of the local magnetic field. Fig. 3 compares the ellipsoid fitting results from the raw and calibrated magnetometer data.

TABLE I  
EXPLANATION OF PEDESTRIAN WALKING PATTERNS

ID	Walking pattern explanation
M1	Forward walking
M2	Backward walking
M3	Left lateral walking
M4	Right lateral walking
M5	Running

### C. Coordinate System Transformation

Assuming that the measurements of acceleration gravity and magnetometer are represented as follows, respectively:

$$A_b = [a_b^x \ a_b^y \ a_b^z]^T \quad (2)$$

$$G_b = [g_b^x \ g_b^y \ g_b^z]^T \quad (3)$$

$$M_b = [m_b^x \ m_b^y \ m_b^z]^T \quad (4)$$

where  $a_b^x$ ,  $a_b^y$ , and  $a_b^z$  represent acceleration measurements on the respective axes at the BCS;  $g_b^x$ ,  $g_b^y$ , and  $g_b^z$  represent gravity measurements on the respective axes at BCS; and  $m_b^x$ ,  $m_b^y$ , and  $m_b^z$  represent magnetometer measurements on the respective axes at BCS.

We import the sensor data of magnetometer, accelerometer and gyroscope into AHRS to estimate the smartphone attitude relative to the NCS. Then, we build the rotation matrix  $C_b^n$  according to the quaternion vector updated from AHRS

$$C_b^n = \begin{bmatrix} q_1^2 - q_2^2 - q_3^2 + q_4^2 & 2q_1q_2 - 2q_3q_4 & 2q_1q_3 + 2q_2q_4 \\ 2q_1q_2 + 2q_3q_4 & -q_1^2 + q_2^2 - q_3^2 + q_4^2 & 2q_2q_3 - 2q_1q_4 \\ 2q_1q_3 - 2q_2q_4 & 2q_2q_3 + 2q_1q_4 & -q_1^2 - q_2^2 + q_3^2 + q_4^2 \end{bmatrix}. \quad (5)$$

We utilize the rotation matrix  $C_b^n$  to project the acceleration and magnetometer measurements into NCS by left multiplying the transform matrix

$$A_n = [a_n^x \ a_n^y \ a_n^z]^T = C_b^n A_b = C_b^n [a_b^x \ a_b^y \ a_b^z]^T \quad (6)$$

$$M_n = [m_n^x \ m_n^y \ m_n^z]^T = C_b^n M_b = C_b^n [m_b^x \ m_b^y \ m_b^z]^T. \quad (7)$$

### D. Walking Pattern Recognition Based on Multihead Convolutional Attention Mechanism

Various walking patterns bring challenges for PDR especially for step detection and step length estimation. In this study, we consider more detailed walking patterns and define five elemental walking patterns, as presented in Table I. These walking patterns are usually performed during the process of pedestrian positioning and navigation.

CNNs have proven extremely effective in extracting informative representations of data [56] and multihead attention mechanism enables the presented approach to ignore the irrelevant features and to focus on a subset of pertinent features [57]. To ensure more accurate walking pattern recognition, we incorporated multihead CNNs [58] and multihead attention mechanism [57] for better feature extraction and selection, as shown in Fig. 4. Multihead CNNs are used in the feature extraction process. The multihead attention mechanism

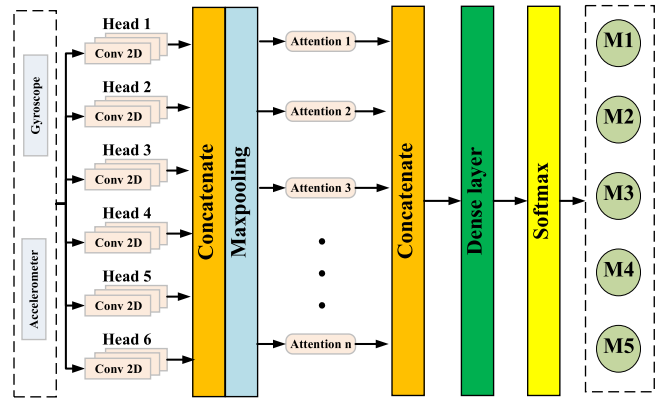


Fig. 4. Walking pattern recognition based on multihead convolutional attention.

supports feature selection. Multihead CNNs can have different filter banks and different processing layers in each head. For example, one head can have a  $4 \times 4$  filter and another head can have a  $7 \times 4$  filter. Additionally, for a certain head, we can even choose whether to have dropout or pooling layers. The multihead CNNs have the unique ability to allocate different feature learning policies to different components of the input signals, which is a promising facet for feature extraction in multichannel time-series signals received from inertial sensors. More details of the multihead CNNs can be found in [58], and more details of the multihead attention mechanism can be found in [57].

The inertial sensor measurements in NCS over a fixed sliding window are expressed as follows:

$$A_i^x = [a_{n,t}^x, a_{n,t+1}^x, \dots, a_{n,t+K-1}^x] \quad (8)$$

$$A_i^y = [a_{n,t}^y, a_{n,t+1}^y, \dots, a_{n,t+K-1}^y] \quad (9)$$

$$A_i^z = [a_{n,t}^z, a_{n,t+1}^z, \dots, a_{n,t+K-1}^z] \quad (10)$$

$$G_i^x = [g_t^x, g_{t+1}^x, \dots, g_{t+K-1}^x] \quad (11)$$

$$G_i^y = [g_t^y, g_{t+1}^y, \dots, g_{t+K-1}^y] \quad (12)$$

$$G_i^z = [g_t^z, g_{t+1}^z, \dots, g_{t+K-1}^z] \quad (13)$$

$$D_i = [A_i^x, A_i^y, A_i^z, G_i^x, G_i^y, G_i^z] \quad (14)$$

where  $D_i$  represents the input vector at time and  $K$  represents the size of the sliding window;  $a^x$ ,  $a^y$ , and  $a^z$  indicate the triaxis accelerometer in NCS; and  $g^x$ ,  $g^y$ , and  $g^z$  indicate the triaxis gyroscope in NCS.

Sensor feature extraction is a key step in recognizing walking patterns. To extract discriminative features, we design a six-head CNN to process the sensor vector. The feature maps of the previous layer are convolved with pretrained convolutional kernels. The  $j$ th feature map at the  $i$ th layer of  $c$ th head is a matrix, and  $v_{ij}^{x,c}$  denotes the value at the  $x$ th row, which is computed as follows:

$$v_{ij}^{x,c} = f_{\text{ReLU}}(f_{\text{conv } 2d}^c(v_{i-1}^{x,p})) \quad \forall c = 1, 2, \dots, 6 \quad (15)$$

where  $f_{\text{ReLU}}$  is the activation function. The convolution function  $f_{\text{conv } 2d}^c$  of the  $c$ th head in the multihead CNN is presented

**Algorithm 1** Walking Pattern Recognition Based on Multihead Convolutional Attention Mechanism

```

1: Input: training data with labeled walking pattern:  $D = \{X_i, Y_i\}$ , test data without labeled walking pattern
2: Output: walking pattern of pedestrian
3: // Initialization
4: Data Normalization
5: Split normalized data set into train (80%,  $D_{train} = \{S_i^{train}, Y_i^{train}\}$ ) and validation (20%,  $D_{val} = \{S_i^{val}, Y_i^{val}\}$ )
6: Initialize parameters  $\theta$ 
7: // Training on training and validation dataset
8: For epoch = 1, M do
9:   For epoch = 1, M do
10:    Get the input signal  $S_i \in D_{train}$ 
11:    Utilize multi-head CNNs to extract feature with equation (15)(16)
12:    Utilize multi-head attention to capture relevant information on different subspaces and highlight the importance of different features with equation (17)-(19)
13:    Get the output walking pattern  $\hat{y}_i$ 
14:    Calculate cost function  $L$  using cross-entropy error function with equation (20)
15:    Perform a gradient decent step on  $(L|\theta)$  to minimize the cost function
16:    If n%20 == 0 do
17:      validate the model using  $D_{val}$ 
18:    End if
19:  End for
20: End for
21: //Online testing
22: Leverage trained model to predict walking pattern of pedestrian
23: End for

```

as follows:

$$f_{conv, 2d}^{c, p}(v_{i-1}^{x+p}) = b_{ij} + \sum_m \sum_{p=0}^{n_i^c-1} w_{ijm}^{p,c} v_{(i-1)m}^{x+p,c} \quad (16)$$

where  $b_{ij}$  is the bias,  $m$  is the index of the feature maps at the  $(i-1)$ th layer,  $w_{ijm}^{p,c}$  is the value of the convolutional kernel at the position  $p$ , and  $n_i^c$  is the size of convolutional kernel at the  $c$ th head  $i$ th layer of the multihead CNN.

After extracting features, a multihead attention mechanism is utilized to capture relevant information on different subspaces and highlight the importance of different features. The multihead attention mechanism relies on scaled dot-product attention, which operates on a query  $Q$ , a set of key–value pairs  $(K, V)$

$$\text{Attention}(Q, K, V) = \text{softmax}\left(\frac{QK^T}{\sqrt{d_k}}\right)V \quad (17)$$

where  $d_k$  is the key dimensionality. In self-attention, query  $Q$  and key–value pairs  $(K, V)$  come from the previous layer output.

To exploit features from different representation subspaces at different positions extracted from different convolution channels, multihead attention is further utilized to obtain  $h$  different representations of  $(Q, K, V)$ , compute scaled dot-product attention for each representation, and concatenate the results. The multihead attention is calculated as

$$\text{MultiHead}(Q, K, V) = \text{Concat}(\text{head}_1, \dots, \text{head}_h)W^0 \quad (18)$$

$$\text{head}_i = \text{Attention}\left(QW_i^Q, KW_i^K, VW_i^V\right) \quad (19)$$

where  $W_i^Q$ ,  $W_i^K$ , and  $W_i^V$  are the parameter matrix in parallel attentions with dimensions  $d_q/h$ ,  $d_k/h$ , and  $d_v/h$ , respectively.  $W^0$  is the output weight matrix with  $d_0$  dimension.

	M1	99.11	0.00	0.03	0.07	0.79
Truth label	M2	0.00	99.53	0.28	0.19	0.00
M3	0.18	0.09	98.54	1.19	0.00	
M4	0.24	0.60	1.16	98.00	0.00	
M5	1.41	0.00	0.07	0.05	98.47	
	M1	M2	M3	M4	M5	

Fig. 5. Performance for walking pattern recognition using the proposed method.

Finally, we choose the cross-entropy error function as cost function and minimize the cost function to train the model

$$\text{loss} = - \sum_i (y_i \log \hat{y}_i + (1 - y_i) \log (1 - \hat{y}_i)) \quad (20)$$

where  $\hat{y}_i$  is the prediction label for the input vector  $D_i$  while  $y_i$  is the ground-truth label.

In this article, we set  $h$  to 30. For each head, we use  $d_q/h = d_k/h = d_v/h = 128$ . The proposed method effectively recognizes pedestrian walking pattern by combining multihead CNN with multihead attention. The pseudocode for the proposed walking pattern recognition method is summarized in Algorithm 1.

Fig. 5 demonstrates the recognition accuracy of the proposed walking pattern recognition method in the form of a confusion matrix. The columns represent the actual performed walking pattern while the rows represent the predicted walking pattern. The principal diagonal reports the correctly classified samples for each walking pattern while the off-diagonal elements report the misclassified samples. Globally, the proposed walking pattern recognition method classified the walking pattern in the correct category more than 98.00%, no matter what walking pattern is performed. The average recognition accuracy of the proposed walking pattern recognition method is 98.73%.

#### E. Step Counting and Step Length Estimation Based on Walking Patterns

Considerable research has been developed to improve the accuracy of step detection, including peak detection [22], finite-state machine [59], autocorrelation [23], and so on. To demonstrate the effect of walking pattern on the step counting performance, we invite 15 pedestrians to walk 100 steps with different walking patterns and estimate the number of steps with different step counting algorithms. Pedestrians repeat each scenario five times. The step counting error rate of each scenario is shown in Fig. 6. All of them achieve superior step detection accuracy in the case of walking forward while all of them achieve poor step-count accuracy in the case of backward walking and lateral walking. The autocorrelation algorithm has stronger robustness among different walking patterns. To achieve accurate step counting in different walking modes,

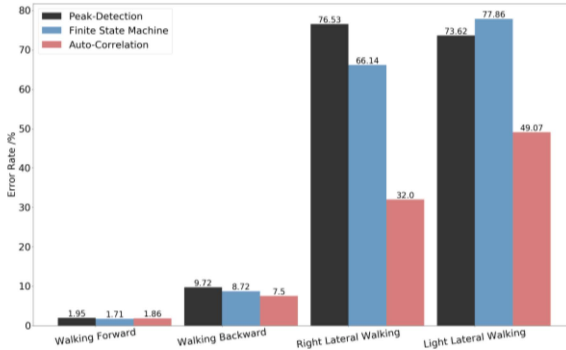


Fig. 6. Step counting error rate of different walking patterns.

we designed an autocorrelation pedometer algorithm based on the walking pattern. The algorithm trains different thresholds according to the walking pattern in the offline stage and adaptively switches the threshold according to the results of walking pattern recognition in the online stage.

The researcher proposed an ocean of step length estimation methods, including geometric relationships, empirical models [28], [29], [60], or deep learning models [31], [33]. However, the step length estimation is very sensitive to the pedestrian's walking pattern. The above-mentioned methods work only well in forward walking situations, but their error overgrows in cases of backward walking, lateral walking, and running. To overcome this challenge, we propose a robust pedestrian step-length estimation method based on walking pattern recognition. We train different step length models for different walking patterns in the offline phase. More info about the step-length model is detailed in our previous work [31], [33]. During the online predicting, we first recognize the walking pattern by the proposed walking pattern method, and then automatically selected the optimal step length model for each walking pattern.

#### F. Hybrid Heading Estimation for Arbitrary Attitude

Since PDR characteristics, the heading estimation significantly affects positioning performance, and it is also the most challenging component of the PDR system. In addition to using PCA to solve attitude problems, we use multisource fusion methods to enhance the accuracy and robustness of heading estimation, as shown in Fig. 7.

1) *Local Walking Direction Estimation Using Acceleration and Magnetic Field*: Denoting gravity vector at NCS as a  $3 \times 1$  vector  $G_n = [0 \ 0 \ 9.81]^T$ , we project the acceleration and magnetometer measurements into the horizontal plane as follows:

$$A_n^{\text{hor}} = A_n - \left( \frac{A_n \bullet G_n}{G_n \bullet G_n} \right) G_n \quad (21)$$

$$M_n^{\text{hor}} = M_n - \left( \frac{M_n \bullet G_n}{G_n \bullet G_n} \right) G_n. \quad (22)$$

The smartphone attitude continually changes, and the offset between pedestrian walking direction and device direction is not constant. Based on the fact that the largest variations of the horizontal acceleration component are parallel to the pedestrian's walking direction, the first eigenvector is regarded as

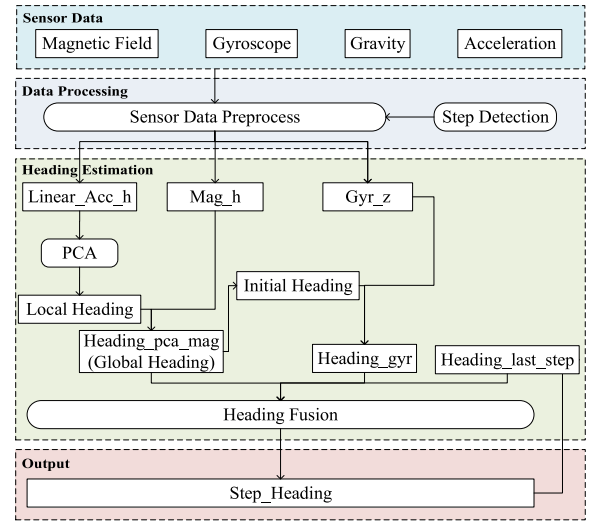


Fig. 7. Pedestrian heading estimation.

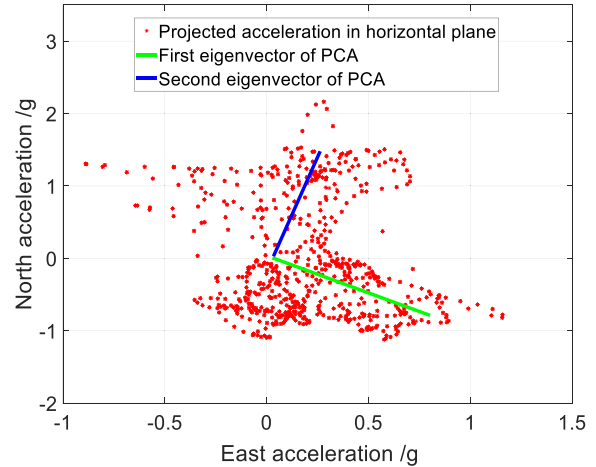


Fig. 8. Eigenvector extraction based on PCA.

the heading of pedestrian [37]. Therefore, we leverage PCA to extract the local walking direction by computing the first eigenvector, as shown in Fig. 8.

The heading angle  $\theta_{\text{Mag}}$  is the intersection angle between the first eigenvector  $\text{mobOri}$  and the horizontal component of magnetism at NCS, which is calculated by vector dot product

$$\theta_{\text{Mag}} = \arccos \left( \frac{M_n^{\text{hor}} \bullet \text{mobOri}}{|\text{mobOri}| \bullet |\text{mobOri}|} \right). \quad (23)$$

The estimated heading from PCA cannot distinguish the actual motion heading ( $\theta$ ) and negative heading ( $\theta + 180$ ). To distinguish this ambiguity, we leverage the orientation angle ( $\varphi$ ) from the compass as a reference and choose the PCA heading that is closest to  $\varphi$ . Due to local magnetic field perturbation, heading estimation from magnetism exists significant perturbation in the short term while heading estimation is relatively stable in the long term. To enhance the robustness of heading estimation, we apply a sliding window over the estimated heading angle.

2) *Relative Heading Estimation Using Angular Rate*: We estimate the relative heading of the smartphone via numerical integration of angular rates data from the gyroscope. The angular rate  $\omega_b$  of the smartphone embedded gyroscope is at BCS. We obtain the angular rate  $\omega_n$  at the NCS by left multiplying the rotation matrix  $C_b^n$ .

Since, the raw gyroscope measurement  $\omega_n$  contains bias errors  $b_{gyr}$  that needs to compensate before numerical integration. The compensated angular rate  $\bar{\omega}_n^z$  around the  $z$ -axis can be represented as follows:

$$\bar{\omega}_n^z = \omega_n^z - b_{gyr}^z \quad (24)$$

where  $\omega_n^z$  is the angular rate around the  $z$ -axis at NCS and  $b_{gyr}^z$  is the bias errors around the  $z$ -axis.

The relative heading is obtained by the integral operation of the compensated angular rate

$$\theta_{Gyr}(tf) = \theta_{Gyr}(ts) + \int_{ts}^{tf} \bar{\omega}_n^z(t) dt \quad (25)$$

where  $[ts, tf]$  is the time interval and  $\theta_{tf} - \theta_{ts}$  is heading angle changes in radians at time interval  $[ts, tf]$ . Note that the heading changes relative to the initial orientation. We calculate the absolute heading estimation of the gyroscope by adding the initial heading from the magnetometer with the relative heading from the gyroscope.

3) *Heading Fusion*: Gyroscope provides short-term accurate heading estimation while magnetometer provides long-term coarse heading estimation without accumulative errors. Based on the above characteristics, to obtain a more accurate and stable heading estimation, we fuse previous step heading, magnetometer heading, and gyroscope heading according to the magnetometer variation as well as the correlation between gyroscope and magnetometer. The pedestrian heading is fused as follows:

$$\theta^k = \begin{cases} \alpha\theta^{k-1}, & \theta_{\Delta,c} > \theta_c, \theta_{\Delta,m} \leq \theta_m \\ \alpha\theta^{k-1} + \gamma\theta_{Gyr}^k, & \theta_{\Delta,c} > \theta_c, \theta_{\Delta,m} > \theta_m \\ \beta\theta_{Mag}^k + \gamma\theta_{Gyr}^k, & \theta_{\Delta,c} \geq \theta_c, \theta_{\Delta,m} > \theta_m \\ \alpha\theta^{k-1} + \beta\theta_{Mag}^k + \gamma\theta_{Gyr}^k, & \theta_{\Delta,c} \leq \theta_c, \theta_{\Delta,m} \leq \theta_m \end{cases}$$

$$\theta_{\Delta,c} = |\theta_{Mag}^k - \theta_{Gyr}^k|, \quad \theta_{\Delta,m} = |\theta_{Mag}^k - \theta_{Mag}^{k-1}| \quad (26)$$

where  $\theta_{Mag}^k$  and  $\theta_{Gyr}^k$  represent the heading acquired by the magnetometer and gyroscope for the  $k$ th step, respectively.  $\alpha$ ,  $\beta$ , and  $\gamma$  represent the weighting coefficients of the previous step heading  $\theta^{k-1}$ , magnetometer heading  $\theta_{Mag}^k$ , and gyroscope heading  $\theta_{Gyr}^k$ , respectively. The thresholds  $\theta_c$  and  $\theta_m$  are used to determine the correlation  $\theta_{\Delta,c}$  between magnetometer and gyroscope, and magnetometer variation  $\theta_{\Delta,m}$ .

4) *Heading Outlier Filtering*: There should be no significant change in the heading estimation results of neighbor steps during normal walking without significant turning [41]. However, unexpectedly rotating or shaking a smartphone arouses marked heading fluctuation, but no turning event. To restrain the heading fluctuation caused by unexpected hand movements, we describe a postprocessing outlier filtering algorithm by analyzing the heading different values between adjacent steps. If the current step heading is significantly larger (smaller) than the heading of the previous step

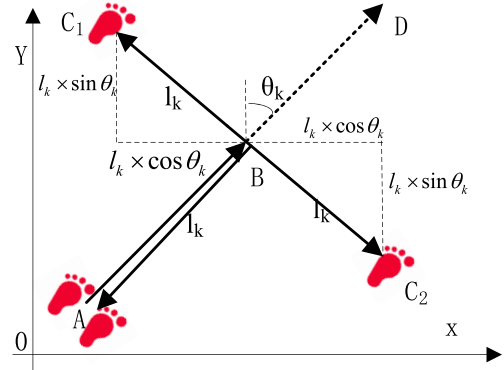


Fig. 9. Pedestrian position update.

and smaller (larger) than the heading of the next step, and both two difference values beyond related threshold values, the heading estimation result of the current step is regarded as an outlier. Then, we calibrate the heading of the pedestrian by averaging the heading of the previous and next steps.

#### G. Position Update According to Walking Patterns

For forward walking situations, traditional PDR effectively estimates the real-time heading of the pedestrian. However, for backward walking or lateral walking situation, the heading angle or pedestrian remains forward, thus resulting in the reckoning trajectory will continue updating forward that is perpendicular or opposite to the actual trajectory. As shown in Fig. 9, in the case of backward walking, the pedestrian walks from starting point A to point B, and then back to starting point A. The final pedestrian trajectory reckoned by the traditional PDR method is  $A \rightarrow B \rightarrow D$ , which is opposite to the pedestrian truth trajectory. In the case of either left or right lateral walking, the pedestrian walks from starting point A to point B, and then laterally walks from B to point  $C_1$  ( $C_2$ ). The final pedestrian trajectory reckoned by the traditional PDR method is still  $B \rightarrow D$ , which is perpendicular to the pedestrian truth trajectory. Therefore, backward walking or lateral walking will cause an enormous cumulative error.

To address this issue, we define the pedestrian positioning equation as follows:

$$\begin{cases} x_k = x_{k-1} + \alpha_k l_k \times \sin \theta_k + \beta_k l_k \times \cos \theta_k \\ y_k = y_{k-1} + \alpha_k l_k \times \cos \theta_k - \beta_k l_k \times \sin \theta_k \end{cases} \quad (27)$$

where  $(x_k, y_k)$  represents the pedestrian locations in NCS at the  $k$ th step.  $l_k$  and  $\theta_k$  represent the step length and heading of pedestrian, respectively.  $\alpha_k$  and  $\beta_k$  are the flag of detected walking patterns. In the case of forward walking,  $\alpha_k$  is set to 1 and  $\beta_k$  is set to 0. In the case of backward walking,  $\alpha_k$  is set to -1 and  $\beta_k$  is set to 0. In the case of left lateral walking,  $\alpha_k$  is set to 0 and  $\beta_k$  is set to -1. In the case of right lateral walking,  $\alpha_k$  is set to 0 and  $\beta_k$  is set to 1. Compared with the traditional PDR method, the proposed position updating method based on walking pattern recognition effectively decreases the positioning error caused by backward walking or lateral walking.

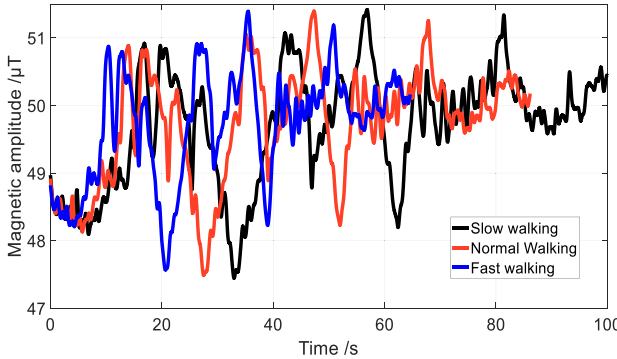


Fig. 10. Magnetic amplitude of different walking speeds.

#### H. Improved PDR Performance With Online Magnetic Fingerprint Trajectory Calibration

Since acceleration and gyroscope drifts, PDR suffers from localization error accumulated with time caused by the inaccurate step counting, step length, heading, and position estimation. The performance of PDR may dramatically degrade over a relatively short period. To restrain the PDR accumulative error, we proposed a novel location calibration method based on a magnetic field that is ubiquitous and does not depend on any additional infrastructure. We utilize the magnetic signals gathered from a smartphone for pedestrian trajectory calibration.

*1) Forward and Backward Magnetic Fingerprint Trajectory:* The ambiguity of magnetism's magnitude in an open area may result in obvious positioning error. To enhance the discernibility of the magnetic field, we build a 3-D attitude-free magnetic field sequence model, which leverages pedestrian motion information to vectorize several magnetic field measurements to form a higher discernibility location signature.

When a pedestrian performs PDR, the magnetic information is automatically collected in passing. The collected attitude-free magnetic field sequences are associated with the position of performing PDR. We call the key-value pairs of the magnetic field information and the corresponding position obtained online as an online magnetic fingerprint trajectory. Collecting the direction of the magnetic fingerprint is consistent with the pedestrian walking direction, which we call forward magnetic fingerprint trajectory. Forward magnetic fingerprint trajectory matching calibration achieves accurate calibration result only when the pedestrian walks along the same path in the same direction once again. To extend the matching calibration probability, we generate the backward magnetic fingerprint trajectory by reversing the forward magnetic fingerprint trajectory for the reverse movement along the path (e.g., coming back). Online collected forward and backward magnetic fingerprint trajectories are stored in the smartphone and used for calibrating the accumulative errors of the subsequent PDR in the form of matching localization.

*2) Magnetic Fingerprint Trajectory Matching Based on Dynamic Time Warping:* As shown in Fig. 10, the magnetic amplitude collected by the pedestrian suffers from the spatial sampling density variation issue, due to both varying walking

speed and sensor sampling frequency. Fortunately, dynamic time warping (DTW) [61] can align and quantify the similarity of two trajectories with different spatial sampling densities [7]. Classical DTW requires that the input signal is 1-D. A simple method is to utilize the magnetic amplitude as the input signal of DTW, and the DTW distance ( $D$ ) is expressed as

$$D(i, j) = d(i, j) = \min([D(i-1, j), D(i-1, j-1), D(i, j-1)]) \quad (28)$$

$$d(i, j) = (m_{\text{mea}}(i) - m_{\text{db}}(j))^2 \quad (29)$$

where  $m_{\text{mea}}(i)$  and  $m_{\text{db}}(j)$  represent the  $i$ th measured magnetic amplitude and the  $j$ th magnetic amplitude stored in smartphone, respectively.  $d$  represents the square of the Euclidean distance between the magnetic amplitude pairs of  $m_{\text{mea}}$  and  $m_{\text{db}}$ .

To effectively leverage 3-D magnetic field information, we design a 3DDTW. Based on the idea of dynamic programming, the 3DDTW distance function is equal to the current minimum distance plus the distance of the previous moment, as (30), as follows:

$$D(i, j, k) = d(i, j, k) + \min([D(i-1, j, k), D(i, j-1, k), D(i, j, k-1), D(i-1, j-1, k), D(i, j-1, k-1), D(i-1, j, k-1), D(i-1, j-1, k-1)]) \quad (30)$$

$$d(i, j, k) = (m_{\text{mea}}(k, i) - m_{\text{db}}(k, j))^2 \quad (31)$$

where  $m_{\text{mea}}(k, i)$  and  $m_{\text{db}}(k, j)$  represent the measured attitude-free 3-D magnetic fingerprint and the attitude-free 3-D magnetic fingerprint stored in smartphone, respectively.  $d$  represents the square of the Euclidean distance between the magnetic amplitude pairs of  $m_{\text{mea}}$  and  $m_{\text{db}}$ .  $D(i-1, j, k)$ ,  $D(i, j-1, k)$ ,  $D(i, j, k-1)$ ,  $D(i-1, j-1, k)$ ,  $D(i, j-1, k-1)$ ,  $D(i-1, j, k-1)$ , and  $D(i-1, j-1, k-1)$  are the 3DDTW distances at the previous moment in the 3-D coordinate system.

*3) Online Magnetic Fingerprint Trajectory Calibration:* Magnetic fingerprint trajectory matching with high similarity means that the pedestrian is walking on a historical path. Once a perfect matching result is obtained, we calibrate the heading and replace the current locations with the locations of the matched magnetic fingerprint trajectory. The reason to use the locations of matched magnetic fingerprint trajectory as the calibration reference locations is that PDR localization errors accumulated with time. Therefore, replacing the latest PDR location and heading with the locations and heading of earlier fingerprint trajectory if there exists a perfect matching result is an effective way to restrain accumulative errors of PDR. Fig. 11 illustrates the procedure of online magnetic fingerprint trajectory calibration based on forward and backward magnetic fingerprint trajectory matching. Fig. 12 demonstrates the effect of the online magnetic fingerprint trajectory calibration on the improvement of positioning accuracy.

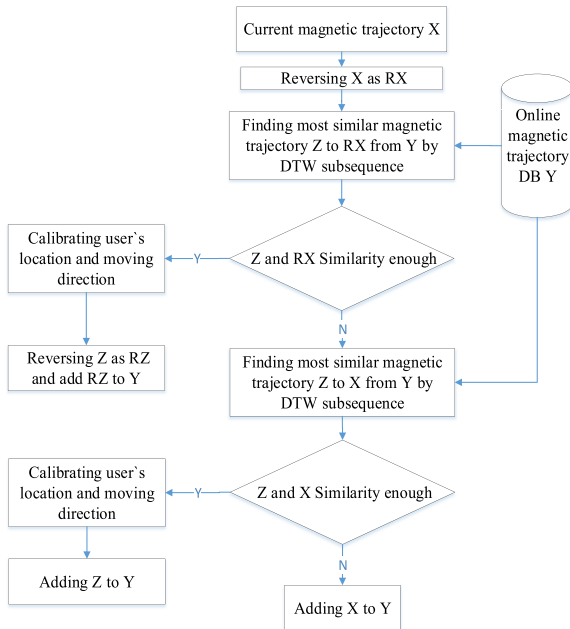


Fig. 11. Flowchart of online trajectory calibration based on forward and backward magnetic fingerprint trajectories.

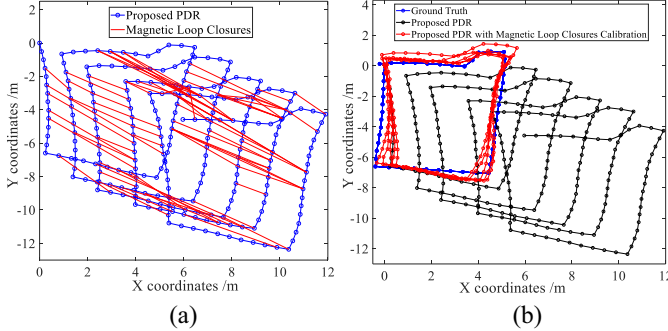


Fig. 12. Improving PDR performance with online magnetic fingerprint trajectory calibration. (a) Magnetic loop closures. (b) Trajectory calibration.

### I. Framework of Proposed Localization

The detailed process of our proposed PDR based on walking pattern recognition and online magnetic trajectory calibration is presented in Algorithm 2.

## IV. EXPERIMENTATION AND EVALUATION

In this section, we thoroughly evaluate the proposed method. The experimental setup is first described. Then, various experiments are conducted in indoor and outdoor scenarios, and the accuracy of the proposed PDR method is verified by comparing it with the ground truth from a foot-mounted IMUs module. Sections IV-B and IV-C evaluate the impact of the walking pattern and online magnetic fingerprint trajectory calibration on localization accuracy, respectively. Positioning accuracy of the proposed PDR method under typical PDR scenarios is analyzed in Section IV-D. Section IV-E compares the proposed method with state-of-the-art methods.

### A. Experimental Setup

To evaluate the proposed PDR method based on walking pattern recognition and online magnetic fingerprint trajectory

### Algorithm 2 PDR Based on Walking Pattern Recognition and Online Magnetic Fingerprint Trajectory Calibration

```

1: Input: sensor data
2: Output: localization of pedestrian
3: Transform acceleration and magnetic from BCS to NCS with equation (5)-(7)
4: Step event detection
5: For each step do
6:   Recognize walking pattern with multi-head convolutional attention network
7:   Adaptively adjust parameters of step counting and step length estimation according to walking patterns
8:   //heading estimation
9:   Local walking direction estimation with equation (21)-(23)
10:  Relative Heading Estimation with equation (24)(25)
11:  Heading fusion with equation (26)
12:  Position update according to walking pattern with equation (27)
13: //Online trajectory calibration
14:  Collect magnetic fingerprint during performing PDR
15:  Generate forward and backward magnetic fingerprint trajectory
16:  Magnetic fingerprint trajectory matching with equation (30)-(31)
17:  Calibrate position and moving direction of pedestrian
18: End for

```

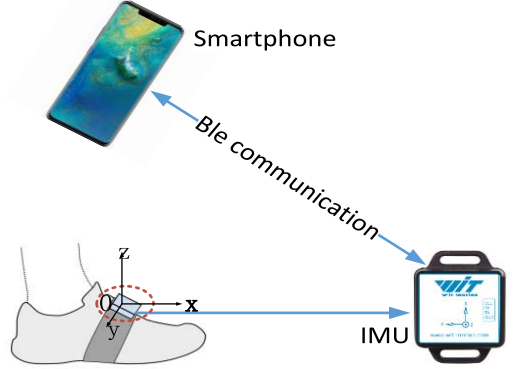


Fig. 13. Devices used in experiments.

calibration, we carried out experiments in an indoor office, shopping malls, subway station, streets, and pedestrian skyway. Mate 9 from Huawei Inc. is used for experiments, which built-in nine-DoF sensors [a three-axis accelerometer and gyroscope from InvenSense (ICM-20690) and a three-axis magnetometer (amk09911)], with 8 core 2.4-GHz processor. The experimental data are sampled at a frequency of 100 Hz.

A foot-mounted inertial navigation system (INS) aided by the zero velocity update (ZUPT), zero angular rate update (ZARU), and magnetic angular rate update (MARU) technologies has the ability to constraint the accumulative errors and achieves a 0.3% horizontal positioning accuracy on the traveled distance [62]. Additionally, INS can provide more high frequency. Therefore, foot-mounted INS is the best way to evaluate the positioning performance of the PDR system. As illustrated in Fig. 13, the performance evaluation system consists of an Android smartphone and a foot-mounted INS module (MPU9250 [63] from Invensense Company, Ltd, San Jose, CA, USA). The precise pedestrian position from the foot-mounted INS module is sent to the smartphone via Bluetooth and synchronizes with the measurements of smartphone-embedded MEMS sensors.

We use the estimated total traveled distance (TTD), step detection rate (SDR), step length error (SLE), and circular

TABLE II  
DESCRIPTION OF VOLUNTEERS

Subject	Gender	Age	Height (cm)	Weight (kg)	Speed
S1	M	27	171	68	Fast/slow
S2	M	26	183	82	Fast
S3	F	23	155	45	Normal
S4	M	35	192	85	Fast/normal
S5	F	25	161	54	Fast/slow
S6	F	27	158	57	Fast/normal
S7	M	31	175	70	Fast
S6	F	57	162	49	Slow/normal
S7	M	71	167	67	Slow

Slow (around 0.83 m/s), normal (around 1.4 m/s), fast (around 2.5 m/s)

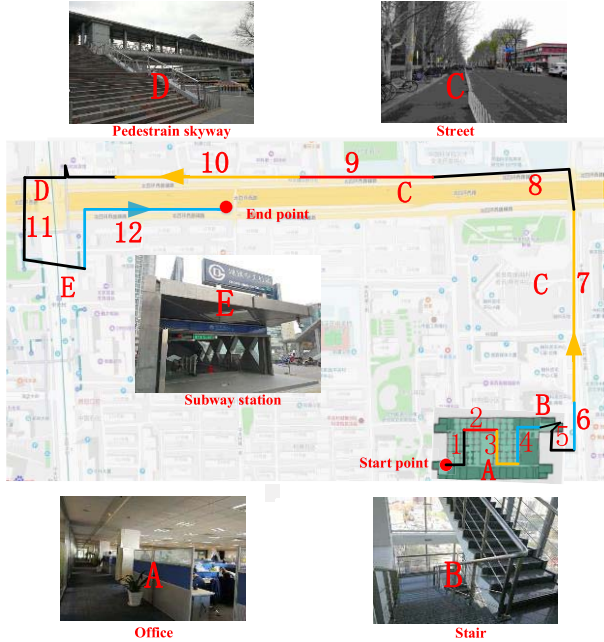


Fig. 14. Preplanned paths description. The volunteer walked along the highlighted curve with the corresponding walking pattern.

error probability (CEP) to quantify the performance of PDR. We invited a group of heterogeneous volunteers to evaluate the proposed method. Table II details the volunteers' information.

#### B. Improving PDR Performance With Walking Pattern Recognition

We carried out a long-distance walking experiment to verify how much performance improvement the walking pattern recognition brings to the proposed PDR method. We started walking from an indoor office. We walked downstairs, left the office, and walked along the preplanned path to my dormitory. Fig. 14 illustrates the entire paths. Volunteers made a 1569 s (26.15 min) walk covering office, indoor stair, street, pedestrian skyway, and subway station. To facilitate the evaluation, we randomly divided the preplanned paths into 12 segments (see Fig. 14) set mark points at each split point. The corresponding walking pattern is detailed in Table III. During the experiment, volunteers precisely walked along the entire preplanned paths with the corresponding walking pattern. Volunteers only change their walking pattern at each

split point. A total number of 2400 steps are taken in the preplanned paths. The proposed PDR with walking pattern recognition successfully detected 2438 steps with 98.42% accuracy while the proposed PDR without walking pattern recognition successfully detected 1776 steps with 74% accuracy. The ground-truth walking distance is 1615.18 m. When reached the endpoint, the final position error of the proposed PDR with walking pattern recognition is 56.34 m, 3.49% over ground-truth walking distance, while the final position error of the proposed PDR without walking pattern recognition is 595.57 m, 36.87% over ground-truth walking distance.

Table III summarizes the recognition accuracy of each segment walking pattern. The performance comparison of PDR with walking pattern recognition and without walking pattern recognition is detailed in Table IV. As expected, the walking pattern recognition significantly improves the PDR performance, and the SDR, SLE, CEP (50%), CEP (75%), and CEP (95%) are 98.42%, 4.6 cm, 3.6 m, 6.72 m, and 11.87 m, respectively. Compared to PDR without walking pattern recognition, the performance of PDR with walking pattern recognition was enhanced by 24.42%, 4.8 cm, 116.97 m, 252.75 m, and 466.79 m in SDR, SLE, CEP (50%), CEP (75%), and CEP (95%). The proposed PDR method enhances the localization accuracy by adaptively adjusting the parameters of step detection, step length model, heading model, and position update according to the walking pattern recognition results.

To further verify the robustness of the walking pattern recognition algorithm, we supplement the experiment of frequently switching walking pattern in a small-scale space. Volunteers change walking patterns every 8–10 m (10–15 steps). The average walking pattern recognition accuracy drops to 91.8%. The main reason for recognition accuracy descension is that the test window near the walk pattern switching point contains sensor data on two different walking patterns, which bring more challenges for walking pattern recognition. Fortunately, in practical application, it is very rare to switch walking patterns frequently in small-scale spaces.

#### C. Improving PDR Performance With Online Magnetic Fingerprint Trajectory Calibration

To evaluate the online magnetic fingerprint matching calibration performance, we experimented on planned round-trip routes in the office and shopping mall. The office is characterized by narrow and regular corridors while the shopping mall is characterized by wider and irregular walking paths.

The performance comparison of PDR with online trajectory calibration and without online trajectory calibration is detailed in Table V and Fig. 15. Fig. 15 shows the cumulative distribution function (CDF) of our proposed PDR method in 13 offices and shopping malls, respectively. For the office scenario, the 80 percentile of calibrated localization error is less than 1.62 m while that of uncalibrated localization error is 2.73 m. For the shopping mall scenario, the 80 percentile of calibrated localization error is less than 1.75 m while that of uncalibrated localization error is 2.82 m. As expected, online trajectory calibration significantly improves PDR performance. The experimental results demonstrate that although step detection and step length estimation cannot be

TABLE III  
ACCURACY OF WALKING PATTERN RECOGNITION IN DIFFERENT SEGMENTS

Scenarios	Forward walking				Backward walking		Left lateral walking		Right lateral walking		Running	
Segment	1	5	8	11	2	9	3	7	4	12	6	10
Accuracy (%)	99.2				99.6		97.3		97.5		98.7	

TABLE IV  
PERFORMANCE COMPARISON OF PDR WITH WALKING PATTERN RECOGNITION AND NO WALKING PATTERN RECOGNITION

Methods	TTD	SDR	SLE	CEP (50%)	CEP (75%)	CEP (95%)
Proposed PDR with walking pattern recognition	1583.64 m	98.42%	4.6 cm	3.64 m	6.72 m	11.87 m
Proposed PDR without walking pattern recognition	1163.38 m	74%	9.4cm	120.61 m	259.47 m	478.66 m

TABLE V  
PERFORMANCE COMPARISON OF PDR WITH ONLINE TRAJECTORY CALIBRATION AND NO ONLINE TRAJECTORY CALIBRATION

Scenarios	Methods	SDR	SLE	CEP (50%)	CEP (75%)	CEP (95%)
Office	Proposed PDR with online magnetic fingerprint trajectory calibration	99.21 %	4.3 cm	0.93 m	1.50 m	2.50 m
	Proposed PDR without online magnetic fingerprint trajectory calibration	99.21 %	4.3 cm	1.43 m	2.45 m	4.55 m
Shopping mall	Proposed PDR with online magnetic fingerprint trajectory calibration	98.67 %	4.5 cm	0.89 m	1.58 m	2.69 m
	Proposed PDR without online magnetic fingerprint trajectory calibration	98.67 %	4.5 cm	1.48 m	2.48 m	5.60 m

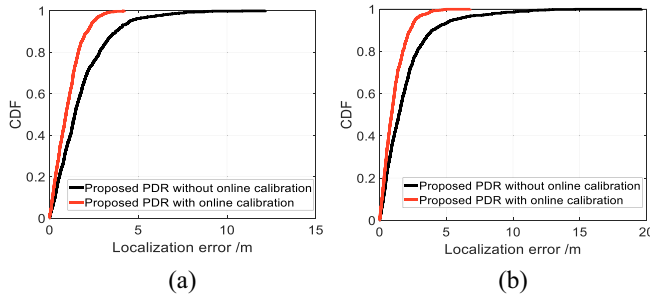


Fig. 15. Performance comparison of PDR with walking pattern recognition and no walking pattern recognition. (a) Office. (b) Shopping mall. Positioning accuracy in typical scenarios.

improved, the online trajectory calibration effectively reduces the positioning error caused by accumulative error and heading estimation error by correcting the position and heading of the pedestrian with opportunistic online magnetic fingerprint trajectory matching.

#### D. Positioning Accuracy in Typical Scenarios

To evaluate the positioning accuracy and robustness of the proposed PDR method, we carried out closed-loop experiments in three typical scenarios: 1) closed rectangular (traveled distance: 100 m); 2) outdoor stadium (traveled distance: 400 m); and 3) intricate path (traveled distance: 210 m), by calculating the distance between the start point and end point. Fig. 16 shows walking trajectories estimated by the proposed method. The final position error over the total traveled distance of the three scenarios is 2.33%, 1.66%, and 2.09%, respectively. Table VI lists detailed experimental results. Statistical results show that the mean of SDR, SLE, CEP (50%), CEP (75%), and CEP (95%) of the proposed method in typical scenarios is 98.73%, 4.4 cm, 0.66 m, 1.13 m, and 2.18 m, respectively.

#### E. Comparing With Other Methods

To justify the superiority of our proposed PDR based on walking pattern recognition and online magnetic fingerprint trajectory calibration, we compared the proposed method with the following PDR methods in terms of CDF.

- 1) Traditional PDR utilizes step detection based on zero crossing, step length estimation based on the relationship of acceleration variance and step frequency, and the yaw angle from Android's compass to reckon the locations of the pedestrian.
- 2) SmartPDR [36] proposes a hybrid heading estimation method that fuses previous heading estimation, gyroscope heading, and magnetic heading based on the variation of magnetometer measurements as well as the correlation between gyroscope measurements and magnetometer measurements. This PDR solution requires pedestrian keeping smartphone on hand all the time.
- 3) RMPCA [40] utilizes rotation matrix and PCA to accurately estimate pedestrian heading, getting rid of the constraints of fixed smartphone attitude.
- 4) Wang *et al.* [37] utilized PCA on global accelerations (PCA-GAs) to estimate pedestrian heading as well as recognized four motion states (walking, upstairs, downstairs, and running) to adaptive adjust parameters of step detection and step length estimation.

We compared the overall localization accuracy of the proposed method and that of mentioned above methods in different walking patterns. To make a fair comparison, we maintain the same walking path, walking pattern, and holding smartphone attitude for each comparison to validate the performance of different methods. Fig. 17 shows the cumulative error distribution of different methods in corresponding walking patterns. With respect to forward walking, 75th percentile positioning accuracy of the proposed PDR method is 2.28 m while those of traditional PDR, SmartPDR, RMPCA,

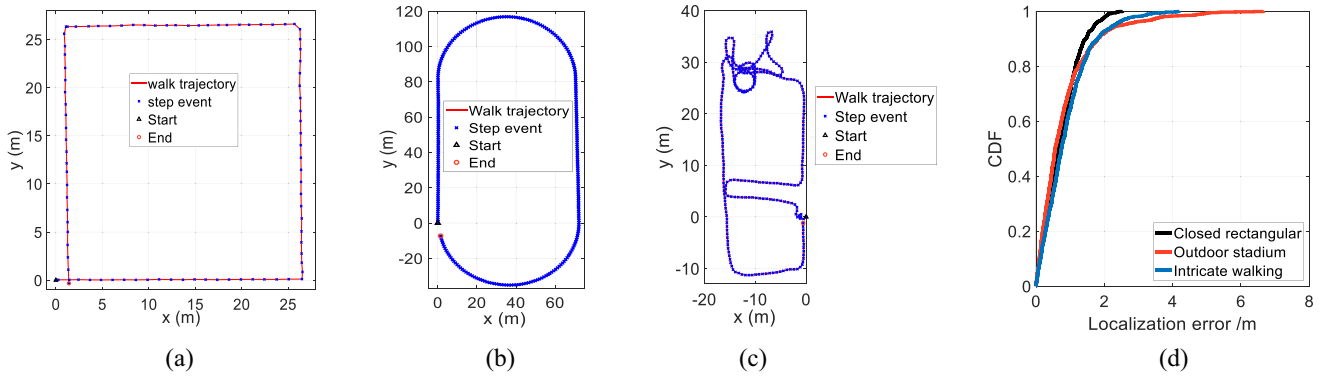


Fig. 16. Walking trajectories estimation in three typical scenarios. (a) Closed rectangular (100 m). (b) Outdoor stadium (400 m). (c) Intricate path (210 m). (d) CDF of three scenarios.

TABLE VI  
EXPERIMENTAL RESULTS OF THREE TYPICAL SCENARIOS

Scenarios	SDR	SLE	CEP (50%)	CEP (75%)	CEP (95%)
Closed rectangular	99.19%	4.3 cm	0.66 m	1.06 m	1.71 m
Outdoor stadium	98.83%	4.4 cm	0.59 m	1.08 m	2.31 m
Intricate path	98.17%	4.5 cm	0.74 m	1.22 m	2.53 m
Mean	98.73%	4.4 cm	0.66 m	1.13 m	2.18 m

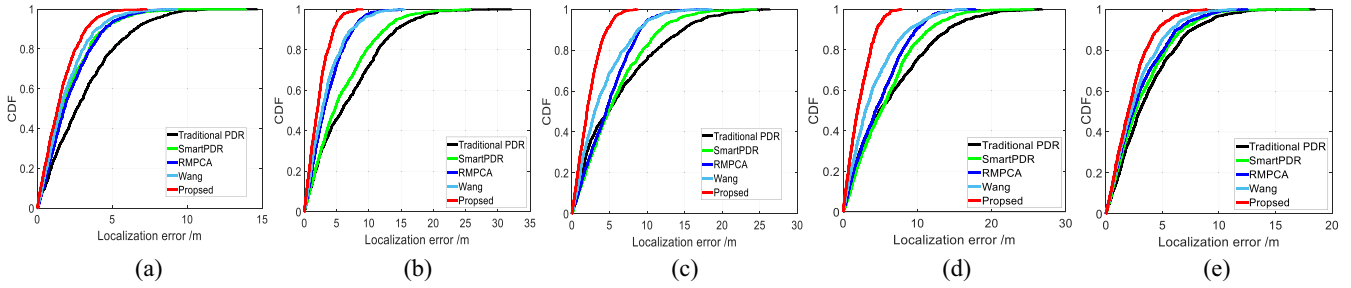


Fig. 17. Comparison with other methods. (a) Forward walking. (b) Backward walking. (c) Left lateral walking. (d) Right lateral walking. (e) Running.

and Wang are 4.49, 3.15, 3.21, and 2.76 m, respectively. Although pointing of the smartphone is consistent with walking heading under running pattern, the performance of all methods is degraded, compared to forward walking. As shown in Fig. 17, the traditional PDR and SmartPDR exist much larger errors, which are not suitable for backward walking, left lateral walking, or right lateral walking scenarios. Since, PCA-based heading estimation, RMPCA, and Wang are more robust against different walking patterns than the traditional PDR and SmartPDR. However, RMPCA and Wang cannot adaptively adjust parameters of step counting and step length estimation for each walking pattern. The cumulative error of all compared methods is not well suppressed. Due to accurate heading estimation for arbitrary attitude, parameters adaptive adjustment of step detection and step length model, and online opportunistic online magnetic fingerprint trajectory calibration, the proposed method achieves promising positioning accuracy.

## V. CONCLUSION

The main issue of the PDR system is that pedestrian usually walks in a variety of walking patterns. Additionally, the heading offset between walking heading and pointing of the smartphone also brings a challenge. In this article, we propose a novel PDR system based on walking pattern recognition and

the online magnetic fingerprint trajectory calibration for pedestrian navigation and positioning using a smartphone. Compared with other PDR methods, the proposed PDR method does not force the pedestrian to walk forward and hold the smartphone in a fixed posture, as well as effectively restrains accumulative errors. We have thoroughly evaluated our proposed PDR method under a variety of experimental scenarios. The experiments have proved that both the walking pattern recognition and online magnetic fingerprint trajectory calibration enhance localization accuracy, and the combination of them yields the best performance. We have enhanced positioning accuracy of the PDR method itself, rather than utilizing the assistance of other auxiliary devices or historical training data. Therefore, the proposed PDR algorithm is not only available for emergency scenarios but also easy to integrate with other positioning technologies to improve positioning accuracy.

Humans are flexible structures, thus resulting in complex and variable movement modes. However, the proposed PDR method only considered five walking patterns (forward walking, backward walking, right lateral walking, left lateral walking, and running). To obtain more accurate location-based services more walking patterns, such as jumping, jogging, sprinting, ascending and descending stairs, crouch walking, and ladder climbing, will be considered in our future work.

## ACKNOWLEDGMENT

The authors would like to thank the editors and the anonymous reviewers for their valuable comments, which greatly improved the quality of this manuscript. Many thanks to the Beijing Key Laboratory of Mobile Computing and Pervasive Device, Institute of Computing Technology, Chinese Academy of Sciences for the support in our research.

## REFERENCES

- [1] *Global Indoor Location-Based Services (LBS) Market Analysis Report*, Grandviewresearch, San Francisco, CA, USA, 2019.
- [2] J. Lai *et al.*, “TagSort? Accurate relative localization exploring RFID phase spectrum matching for Internet of Things,” *IEEE Internet Things J.*, vol. 7, no. 1, pp. 389–399, Jan. 2020.
- [3] K. Yu, K. Wen, Y. Li, S. Zhang, and K. Zhang, “A novel NLOS mitigation algorithm for UWB localization in harsh indoor environments,” *IEEE Trans. Veh. Technol.*, vol. 68, no. 1, pp. 686–699, Jan. 2019.
- [4] N. Yu, X. Zhan, S. Zhao, Y. Wu, and R. Feng, “A precise dead reckoning algorithm based on Bluetooth and multiple sensors,” *IEEE Internet Things J.*, vol. 5, no. 1, pp. 336–351, Feb. 2018.
- [5] R. Wang, Z. Li, H. Luo, F. Zhao, W. Shao, and Q. Wang, “A robust WiFi fingerprint positioning algorithm using stacked denoising autoencoder and multi-layer perceptron,” *Remote Sens.*, vol. 11, no. 11, p. 1293, May 2019.
- [6] H. Zou, Y. Zhou, J. Yang, and C. J. Spanos, “Unsupervised WiFi-enabled IoT device-user association for personalized location-based service,” *IEEE Internet Things J.*, vol. 6, no. 1, pp. 1238–1245, Feb. 2019.
- [7] Q. Wang, H. Luo, A. Men, F. Zhao, and Y. Huang, “An infrastructure-free indoor localization algorithm for smartphones,” *Sensors*, vol. 18, no. 10, p. 3317, Oct. 2018.
- [8] Q. Wang *et al.*, “Light positioning: A high-accuracy visible light indoor positioning system based on attitude identification and propagation model,” *Int. J. Distrib. Sens. Netw.*, vol. 14, no. 2, pp. 1–14, Feb. 2018.
- [9] Y. Shu, C. Bo, G. Shen, C. Zhao, L. Li, and F. Zhao, “Magicol: Indoor localization using pervasive magnetic field and opportunistic WiFi sensing,” *IEEE J. Sel. Areas Commun.*, vol. 33, no. 7, pp. 1443–1457, Jul. 2015.
- [10] Q. Wang, H. Luo, F. Zhao, and W. Shao, “An indoor self-localization algorithm using the calibration of the online magnetic fingerprints and indoor landmarks,” in *Proc. Int. Conf. Indoor Position. Indoor Navig. (IPIN)*, 2016, pp. 1–8.
- [11] W. Shao *et al.*, “Location fingerprint extraction for magnetic field magnitude based indoor positioning,” *J. Sensors*, vol. 2016, pp. 1–16, Jun. 2017.
- [12] D. Liu, S. Guo, Y. Yang, Y. Shi, and M. Chen, “Geomagnetism-based indoor navigation by offloading strategy in NB-IoT,” *IEEE Internet Things J.*, vol. 6, no. 3, pp. 4074–4084, Jun. 2019.
- [13] L. Zhao, H. Huang, X. Li, S. Ding, H. Zhao, and Z. Han, “An accurate and robust approach of device-free localization with convolutional autoencoder,” *IEEE Internet Things J.*, vol. 6, no. 3, pp. 5825–5840, Jun. 2019.
- [14] L. Pei, J. Liu, R. Guinness, Y. Chen, H. Kuusniemi, and R. Chen, “Using LS-SVM based motion recognition for smartphone indoor wireless positioning,” *Sensors*, vol. 12, no. 5, pp. 6155–6175, May 2012.
- [15] C. A. Ronao and S.-B. Cho, “Human activity recognition with smartphone sensors using deep learning neural networks,” *Expert Syst. Appl.*, vol. 59, pp. 235–244, Oct. 2016.
- [16] H. Zhang, Z. Xiao, J. Wang, F. Li, and E. Szczerbicki, “A novel IoT-perceptive human activity recognition (HAR) approach using multihead convolutional attention,” *IEEE Internet Things J.*, vol. 7, no. 2, pp. 1072–1080, Feb. 2020.
- [17] X. Gao, H. Luo, Q. Wang, F. Zhao, L. Ye, and Y. Zhang, “A human activity recognition algorithm based on stacking denoising autoencoder and LightGBM,” *Sensors*, vol. 19, no. 4, p. 947, Feb. 2019.
- [18] K. Chen, L. Yao, D. Zhang, X. Wang, X. Chang, and F. Nie, “A semi-supervised recurrent convolutional attention model for human activity recognition,” *IEEE Trans. Neural Netw. Learn. Syst.*, vol. 31, no. 5, pp. 1747–1756, May 2020.
- [19] A. Saeed, T. Ozcelebi, and J. Lukkien, “Multi-task self-supervised learning for human activity detection,” *Proc. ACM Interact. Mobile Wearable Ubiquitous Technol.*, vol. 3, no. 2, pp. 1–30, Jun. 2019.
- [20] L. Peng, L. Chen, Z. Ye, and Y. Zhang, “AROMA: A deep multi-task learning based simple and complex human activity recognition method using wearable sensors,” *Proc. ACM Interact. Mobile Wearable Ubiquitous Technol.*, vol. 2, no. 2, pp. 1–16, Jul. 2018.
- [21] H. Zhang, W. Yuan, Q. Shen, T. Li, and H. Chang, “A handheld inertial pedestrian navigation system with accurate step modes and device poses recognition,” *IEEE Sens. J.*, vol. 15, no. 3, pp. 1421–1429, Mar. 2015.
- [22] J. Qian, J. Ma, R. Ying, P. Liu, and L. Pei, “An improved indoor localization method using smartphone inertial sensors,” in *Proc. Int. Conf. Indoor Position. Indoor Navig.*, 2013, pp. 1–7.
- [23] J. Santos, A. Costa, and M. J. Nicolau, “Autocorrelation analysis of accelerometer signal to detect and count steps of smartphone users,” in *Proc. Int. Conf. Indoor Position. Indoor Navig. (IPIN)*, 2019, pp. 1–7.
- [24] W. Shao, H. Luo, F. Zhao, C. Wang, A. Crivello, and M. Z. Tunio, “DePedo: Anti periodic negative-step movement pedometer with deep convolutional neural networks,” in *Proc. IEEE Int. Conf. Commun. (ICC)*, 2018, pp. 1–6.
- [25] Q. Wang *et al.*, “Personalized stride-length estimation based on active online learning,” *IEEE Internet Things J.*, vol. 7, no. 6, pp. 4885–4897, Jun. 2020.
- [26] L. E. Diez, A. Bahillo, J. Otegui, and T. Otim, “Step length estimation methods based on inertial sensors: A review,” *IEEE Sens. J.*, vol. 18, no. 17, pp. 6908–6926, Sep. 2018.
- [27] S. Miyazaki, “Long-term unrestrained measurement of stride length and walking velocity utilizing a piezoelectric gyroscope,” *IEEE Trans. Biomed. Eng.*, vol. 44, no. 8, pp. 753–759, Aug. 1997.
- [28] Q. Ladetto, B. M. Terrier, T. Philippe, and Y. Schutz, “On foot navigation? Continuous step calibration using both complementary recursive prediction and adaptive Kalman filtering,” *J. Navig.*, vol. 53, no. 2, pp. 279–285, 2000.
- [29] H. Weinberg, “Using the ADXL202 in pedometer and personal navigation applications,” Anal. Devices, Norwood, MA, USA, Application Notes, 2002.
- [30] T.-N. Do, R. Liu, C. Yuen, M. Zhang, and U.-X. Tan, “Personal dead reckoning using IMU mounted on upper torso and inverted pendulum model,” *IEEE Sens. J.*, vol. 16, no. 21, pp. 7600–7608, Nov. 2016.
- [31] Q. Wang, L. Ye, H. Luo, A. Men, F. Zhao, and C. Ou, “Pedestrian walking distance estimation based on smartphone mode recognition,” *Remote Sens.*, vol. 11, no. 9, p. 1140, May 2019.
- [32] D. Bousdar Ahmed, E. M. Diaz, and J. J. García Domínguez, “Automatic calibration of the step length model of a pocket INS by means of a foot inertial sensor,” *Sensors*, vol. 20, no. 7, p. 2083, Apr. 2020.
- [33] Q. Wang, L. Ye, H. Luo, A. Men, F. Zhao, and Y. Huang, “Pedestrian stride-length estimation based on LSTM and denoising autoencoders,” *Sensors*, vol. 19, no. 4, p. 840, Feb. 2019.
- [34] S. Vandermeeren, H. Bruneel, and H. Steendam, “Feature selection for machine learning based step length estimation algorithms,” *Sensors*, vol. 20, no. 3, p. 778, Jan. 2020.
- [35] S. O. H. Madgwick, A. J. L. Harrison, and R. Vaidyanathan, “Estimation of IMU and MARG orientation using a gradient descent algorithm,” in *Proc. IEEE Int. Conf. Rehabil. Robot.*, 2011, pp. 1–7.
- [36] W. Kang and Y. Han, “SmartPDR: Smartphone-based pedestrian dead reckoning for indoor localization,” *IEEE Sens. J.*, vol. 15, no. 5, pp. 2906–2916, May 2015.
- [37] B. Wang, X. Liu, B. Yu, R. Jia, and X. Gan, “Pedestrian dead reckoning based on motion mode recognition using a smartphone,” *Sensors*, vol. 18, no. 6, p. 1811, Jun. 2018.
- [38] M. Elhoushi, J. Georgy, A. Noureldin, and M. J. Korenberg, “Motion mode recognition for indoor pedestrian navigation using portable devices,” *IEEE Trans. Instrum. Meas.*, vol. 65, no. 1, pp. 208–221, Jan. 2016.
- [39] J. Qian, L. Pei, J. Ma, R. Ying, and P. Liu, “Vector graph assisted pedestrian dead reckoning using an unconstrained smartphone,” *Sensors*, vol. 15, no. 3, pp. 5032–5057, Mar. 2015.
- [40] Z.-A. Deng, G. Wang, Y. Hu, and D. Wu, “Heading estimation for indoor pedestrian navigation using a smartphone in the pocket,” *Sensors*, vol. 15, no. 9, pp. 21518–21536, Aug. 2015.
- [41] Z. Deng, X. Liu, Z. Qu, C. Hou, and W. Si, “Robust heading estimation for indoor pedestrian navigation using unconstrained smartphones,” *Wireless Commun. Mobile Comput.*, vol. 2018, pp. 1–11, Jul. 2018.
- [42] D. Wu, L. Xia, and J. Geng, “Heading estimation for pedestrian dead reckoning based on robust adaptive Kalman filtering,” *Sensors*, vol. 18, no. 6, p. 1970, Jun. 2018.
- [43] Q. Wang *et al.*, “Pedestrian heading estimation based on spatial transformer networks and hierarchical LSTM,” *IEEE Access*, vol. 7, pp. 162309–162322, 2019.

- [44] Z. Chen, Q. Zhu, and Y. C. Soh, "Smartphone inertial sensor-based indoor localization and tracking with iBeacon corrections," *IEEE Trans. Ind. Informat.*, vol. 12, no. 4, pp. 1540–1549, Aug. 2016.
- [45] V. Magnago, L. Palopoli, R. Passerone, D. Fontanelli, and D. Macii, "A nearly optimal landmark deployment for indoor localisation with limited sensing," in *Proc. Int. Conf. Indoor Position. Indoor Navig. (IPIN)*, 2017, pp. 1–8.
- [46] J. Shang, F. Gu, X. Hu, and A. Kealy, "APFiLoc: An infrastructure-free indoor localization method fusing smartphone inertial sensors, landmarks and map information," *Sensors*, vol. 15, no. 10, pp. 27251–27272, Oct. 2015.
- [47] J.-H. Kim and B.-S. Kim, "Autonomous landmark calibration method for indoor localization," *Sensors*, vol. 17, no. 9, p. 1952, Aug. 2017.
- [48] T. Liu, X. Zhang, Q. Li, and Z. Fang, "Modeling of structure landmark for indoor pedestrian localization," *IEEE Access*, vol. 7, pp. 1–1, 2019.
- [49] B. Zhou, Q. Li, Q. Mao, W. Tu, X. Zhang, and L. Chen, "ALIMC: Activity landmark-based indoor mapping via crowdsourcing," *IEEE Trans. Intell. Transp. Syst.*, vol. 16, no. 5, pp. 2774–2785, Oct. 2015.
- [50] F. Hölzke, J. P. Wolff, F. Golałowski, and C. Haubelt, "Low-complexity online correction and calibration of pedestrian dead reckoning using map matching and GPS," *Geo-Spatial Inf. Sci.*, vol. 22, no. 2, pp. 114–127, 2019.
- [51] L. Shen and W. S. Hui, "Improved pedestrian dead-reckoning-based indoor positioning by RSSI-based heading correction," *IEEE Sens. J.*, vol. 16, no. 21, pp. 7762–7773, Nov. 2016.
- [52] X. Wang, M. Jiang, Z. Guo, N. Hu, Z. Sun, and J. Liu, "An indoor positioning method for smartphones using landmarks and PDR," *Sensors*, vol. 16, no. 12, p. 2135, Dec. 2016.
- [53] H. Xia, J. Zuo, S. Liu, and Y. Qiao, "Indoor localization on smartphones using built-in sensors and map constraints," *IEEE Trans. Instrum. Meas.*, vol. 68, no. 4, pp. 1189–1198, Apr. 2019.
- [54] Y. Li, Y. Zhuang, P. Zhang, H. Lan, X. Niu, and N. El-Sheimy, "An improved inertial/WiFi/magnetic fusion structure for indoor navigation," *Inf. Fusion*, vol. 34, pp. 101–119, Mar. 2017.
- [55] J. Fang, H. Sun, J. Cao, X. Zhang, and Y. Tao, "A novel calibration method of magnetic compass based on ellipsoid fitting," *IEEE Trans. Instrum. Meas.*, vol. 60, no. 6, pp. 2053–2061, Jun. 2011.
- [56] Y. LeCun, Y. Bengio, and G. Hinton, "Deep learning," *Nature*, vol. 521, no. 7553, pp. 436–444, May 2015.
- [57] A. Vaswani *et al.*, "Attention is all you need," in *Proc. Adv. Neural Inf. Process. Syst. (NIPS)*, 2017, pp. 5998–6008. [Online]. Available: <https://doi.org/10.1155/2018/5607036>
- [58] M. Canizo, I. Triguero, A. Conde, and E. Onieva, "Multi-head CNN-RNN for multi-time series anomaly detection: An industrial case study," *Neurocomputing*, vol. 363, pp. 246–260, Oct. 2019.
- [59] J. Ruppelt, N. Kronenwett, and G. F. Trommer, "A novel finite state machine based step detection technique for pedestrian navigation systems," in *Proc. Int. Conf. Indoor Position. Indoor Navig. (IPIN)*, 2015, pp. 1–7.
- [60] J. W. Kim, H. J. Jang, D.-H. Hwang, and C. Park, "A step, stride and heading determination for the pedestrian navigation system," *J. Global Position. Syst.*, vol. 3, nos. 1–2, pp. 273–279, Dec. 2004.
- [61] M. Müller, "Dynamic time warping," in *Information Retrieval for Music and Motion*. Berlin, Germany: Springer, 2007. [Online]. Available: [https://link.springer.com/chapter/10.1007%2F978-3-540-74048-3\\_4](https://link.springer.com/chapter/10.1007%2F978-3-540-74048-3_4)
- [62] Y. Gu, Q. Song, Y. Li, and M. Ma, "Foot-mounted pedestrian navigation based on particle filter with an adaptive weight updating strategy," *J. Navig.*, vol. 68, no. 1, pp. 23–38, Jan. 2015.
- [63] MPU9250. Accessed: Apr. 20, 2020. [Online]. Available: <https://invensense.tdk.com/products/motion-tracking/9-axis/mpu-9250/>



**Qu Wang** (Member, IEEE) received the B.S. degree from the School of Software Engineering, Beijing University of Posts and Telecommunications, Beijing, China, in 2013, and the M.S. degree from the University of Chinese Academy of Sciences, Beijing, in 2016. He is currently pursuing the Ph.D. degree with the School of Information and Communication Engineering, Beijing University of Posts and Telecommunications.

His current main interests include location-based services, pervasive computing, computer vision, and machine learning.



**Haiyong Luo** (Member, IEEE) received the B.S. degree from the Department of Electronics and Information Engineering, Huazhong University of Science and Technology, Wuhan, China, in 1989, the M.S. degree from the School of Information and Communication Engineering, Beijing University of Posts and Telecommunications, Beijing, China, in 2002, and the Ph.D. degree in computer science from the University of Chinese Academy of Sciences, Beijing, in 2008.

He is currently an Associate Professor with the Institute of Computer Technology, Chinese Academy of Sciences, Beijing. His main research interests are location-based services, pervasive computing, mobile computing, and Internet of Things.



**Hao Xiong** received the B.S. degree from the School of Software Engineering, Beijing University of Posts and Telecommunications, Beijing, China, in 2019, where he is currently pursuing the M.S. degree.

His current main interests include location-based services, pervasive computing, and machine learning.



**Aidong Men** (Member, IEEE) received the B.S., M.S., and Ph.D. degrees from the Department of Radio Engineering, Beijing University of Posts and Telecommunications, Beijing, China, in 1987, 1990, and 1994, respectively.

From 1994 to 2000, he was an Associate Professor with the Department of Radio Engineering, Beijing University of Posts and Telecommunications, where he has been a Professor with Telecom Engineering College since 2000. He has published over 100 papers in journals and international conferences.

His research interests include multimedia communication, digital TV, and images and speech signal processing and transmission.

Dr. Men is a Fellow of the Chinese Institute of Electronics and China Institute of Communications. He is also an Invited Fellow of the Science and Technology Committee of State Administration of Radio, Film, and Television.



**Fang Zhao** received the B.S. degree from the School of Computer Science and Technology, Huazhong University of Science and Technology, Wuhan, China, in 1990, and the M.S. and Ph.D. degrees in computer science and technology from Beijing University of Posts and Telecommunications, Beijing, China, in 2004 and 2009, respectively.

She is currently a Professor with the School of Software Engineering, Beijing University of Posts and Telecommunications. Her research interests include mobile computing, location-based services, and computer networks.



**Ming Xia** was born in Yiyang, China, in 1987. He is currently pursuing the Ph.D. degree with the School of Electronic and Information Engineering, Beihang University, Beijing, China.

His research interests include motion recognition, pedestrian inertial positioning, wearable sensor-based positioning, and their applications in location-based service applications, especially in the fire-fighting field.



**Changhai Ou** was born in Tongren, China, in 1989. He received the bachelor's degree in computer science and technology from the School of Computer and Information Technology, Beijing Jiaotong University, Beijing, China, in 2013, and the Ph.D. degree in cyber security from the Institute of Information Engineering, Chinese Academy of Sciences (i.e., School of Cyber Security, University of Chinese Academy of Sciences), Beijing, in July 2018.

He is currently a Research Fellow with the Hardware and Embedded Systems Laboratory, School of Computer Science and Engineering, Nanyang Technological University, Singapore. His current research interests include cryptographic hardware and embedded system security, side-channel attacks, machine learning, and privacy preserving.